Future Batteries 2 (2024) 100003

Contents lists available at ScienceDirect

Future Batteries

journal homepage: www.sciencedirect.com/journal/future-batteries

Enhancing prediction accuracy of Remaining Useful Life in lithium-ion batteries: A deep learning approach with Bat optimizer

Shahid A. Hasib [a,*], S. Islam [b], Md F. Ali [b], Subrata. K. Sarker [c], Li Li [c], Md Mehedi Hasan [b], Dip K. Saha [d]

[a] Department of Control & Instrumentation Engineering, King Fahd University of Petroleum & Minerals, Dhahran, 31261, Saudi Arabia
[b] Department of Mechatronics Engineering, Rajshahi University of Engineering & Technology, Bangladesh
[c] School of Electrical and Data Engineering, University of Technology Sydney, Australia
[d] School of Engineering & Informatics, University of Sussex, Brighton, United Kingdom

ARTICLE INFO

Dataset link: https://phm-datasets.s3.amazonaws.com/NASA/5.+Battery+Data+Set.zip

Keywords:
Li-ion battery
Convolutional neural network
Remaining Useful Life prediction
Battery degradation model
Bat based optimization algorithm

ABSTRACT

Remaining Useful Life (RUL) prediction in lithium-ion batteries is crucial for assessing battery performance. Despite the popularity of deep learning methods for RUL prediction, their complex architectures often pose challenges in interpretation and resource consumption. We propose a novel approach that combines the interpretability of a convolutional neural network (CNN) with the efficiency of a bat-based optimizer. CNN extracts battery data features and characterizes degradation kinetics, while the optimizer refines CNN parameters. Tested on NASA PCoE data, our method achieves exceptional results with minimal computational burden and fewer parameters. It outperforms traditional approaches, yielding an **R2-score** of **0.9987120**, an **MAE** of **0.004397067 Ah**, and a low **RMSE** of **0.00656 Ah**. The proposed model outperforms traditional deep learning models, as confirmed by comparative analysis.

Introduction

The proliferation of essential portable equipment such as electric cars, mobile phones, and laptops has significantly increased the usage of lithium-ion batteries (LIBs). This rise in using a large number of LIBs can lead to increased unwanted incidents associated with these batteries. In particular, the malfunction of batteries may lead to the sudden failure of heavy-duty and portable machinery, resulting in substantial financial losses for industries. Consequently, it has become crucial for researchers to concentrate on battery status prediction, management systems, and Remaining Useful Life (RUL) assessment. RUL can be defined as the remaining number of discharging and charging cycles it can undergo before becoming unusable. Predictive approaches for estimating RUL are crucial in determining the battery's remaining effective time and minimizing system downtime by monitoring cell health [1] (see Tables 1 and 2).

LIBs offer several advantages, such as a longer lifetime, high energy density, lightweight design, and low self-discharge rates [2]. These characteristics have contributed to their widespread adoption across various applications. However, ensuring the reliability and usability of LIBs throughout their life cycle requires extensive research in battery management technologies, RUL prediction, and a good understanding of capacity degradation characteristics. This paper explores the current state of the art of RUL prediction for LIBs, considering the growing importance of battery management technologies and the need for an accurate assessment of remaining useful life. In Fig. 1, we provide a step-by-step process of the RUL prediction method for LIBs using a deep learning method. In general, to generate the battery data, the capacity, resistance, temperature, voltage, etc. a LIB cell is run in various operating conditions. During these operations, several side reactions can occur, leading to material aging and capacity degradation. These may lead to battery failure and system malfunctions in certain situations [3]. Therefore, accurate prediction of the RUL of LIBs is crucial for electrical systems to prevent battery failures and mitigate potential unwanted consequences [4,5].

By keeping LIBs operating within safe and ideal temperature ranges, efficient thermal management reduces degradation mechanisms, improves performance, and makes it possible to predict RUL more precisely [6]. To optimize thermal management, a novel diagonal-type cooling channel design for large-format lithium iron phosphate batteries is introduced in [7]. It performs better than previous studies when evaluating parameters such as channel width, coolant temperature, and flow rate. It does, however, point out shortcomings in the model's mechanical and electrochemical reaction assumptions, suggesting directions for further investigation. In order to mitigate performance

* Corresponding author.
E-mail address: shahidhasib586@gmail.com (S.A. Hasib).

https://doi.org/10.1016/j.fub.2024.100003
Received 25 March 2024; Received in revised form 19 May 2024; Accepted 18 June 2024
Available online 24 June 2024

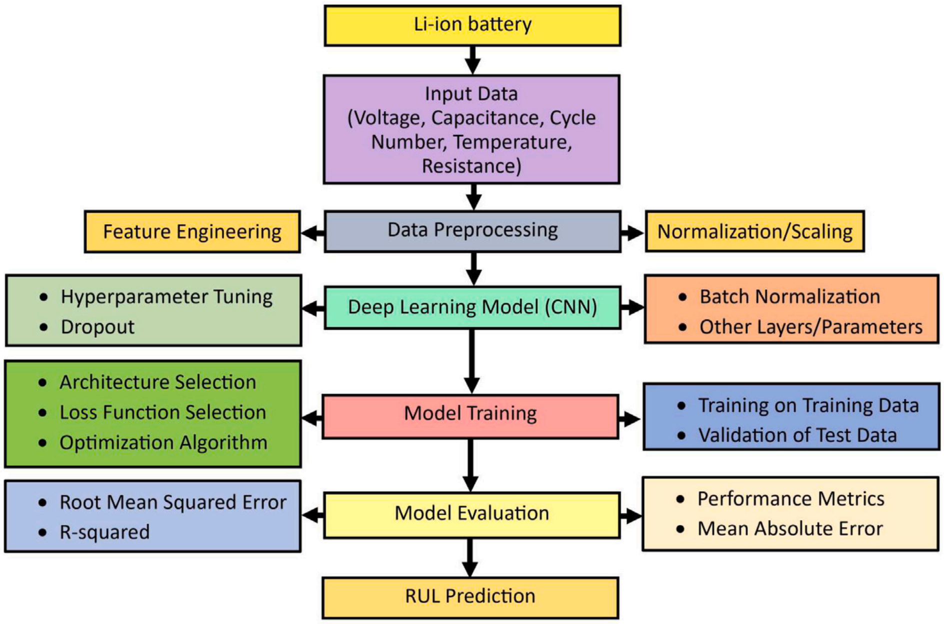

Fig. 1. A deep learning-based approach for RUL prediction of lithium-ion batteries by selecting features: capacity, resistance, temperature, voltage, and reliability tests.

Table 1
Nomenclature.

Symbol	Description
A_i	Loudness of bat i
r_i	Pulse emission rate of bat i
$A_{\min}$	Minimum loudness
$A_{\max}$	Maximum loudness
α	Constant
γ	Constant
Q_κ	Battery capacity at iteration κ
υ	Gaussian noise
σ_1 to σ_7	Variances of random variables
θ_κ	Parameter vector at iteration κ
Q'_κ	Result of CNN degradation model at iteration κ
i	Index for bats
n	Iteration number
κ	Iteration number

Table 2
Abbreviations.

Abbreviation	Definition
AR	Auto Regressive
BA	Bat Algorithm
BMS	Battery Management System
BTMS	Battery Thermal Management System
CAVE	Conditional Variational Auto-Encoder
CALCE	Center for Advanced Life Cycle Engineering
CC	Constant Current
CNN	Convolutional Neural Network
CV	Constant Voltage
EIS	Electrochemical Impedance Spectroscopy
EOL	End-of-Life
EV	Electric Vehicle
ECM	Electrochemical Model
fLsm	Fractional Order Lévy Stable Motion
GNN	Grey Neural Network
HEV	Hybrid Electric Vehicle
HI	Health Indicator
ICS	Incident Command System
LIB	Lithium-ion Battery
LSTM	Long Short-Term Memory
MAE	Mean Absolute Error
MSE	Mean Squared Error
NASA	National Aeronautics and Space Administration
NN	Neural Network
OCV	Open Circuit Voltage
PCM	Phase Change Material
PCoE	Prognostics Center of Excellence
PDF	Probability Density Function
PF	Particle Filter
R2	Coefficient of Determination
RMSE	Root Mean Squared Error
RUL	Remaining Useful Life
RVM	Relevance Vector Machine
SOC	State of Charge
SVM	Support Vector Machine
UKF	Unscented Kalman Filter

degradation caused by high temperatures, the importance of thermal management was highlighted in [8]. Additionally, an analytical algorithm to estimate battery life in vehicle-level testing was also presented. Though useful, it may have drawbacks due to assumptions based on models and the need for more extensive validation in a wider range of operational scenarios and battery chemistries.

To effectively control thermal conductivity errors, especially at high discharging rates, Ref. [9] emphasizes the significance of accurate thermal modeling for electric vehicle battery systems. To optimize vehicle performance and manage batteries efficiently, precise temperature predictions are essential. Still, two important limitations of the study are that it only looked at one type of battery and that more research is needed to apply the results to different battery compositions and operating situations. For preventing thermal runaway (TR) in lithium-ion batteries intended for electric vehicles, Ref. [10] looks into the application of phase change materials (PCMs). The volatile content of PCM implies that even though PCM submersion effectively delays TR triggers, fire propagation may still occur. This suggests that thermal insulation is necessary to stop TR from spreading within battery packs.

The increasing number of publications in various journals related to RUL prediction of LIBs over the past 12 years (2010–2022) is illustrated in Fig. 2(a), and Fig. 2(b) illustrates the publication percentage in prominent journals from 2010 to 2022.

RUL prediction methods can be broadly classified into two categories: data-driven and model-based techniques. Currently, there is a growing trend towards hybrid approaches that combine both data-driven and model-based methodologies [11]. Data-driven approaches leverage historical battery metrics, such as voltage, current, and temperature, along with degradation features. Machine learning methods

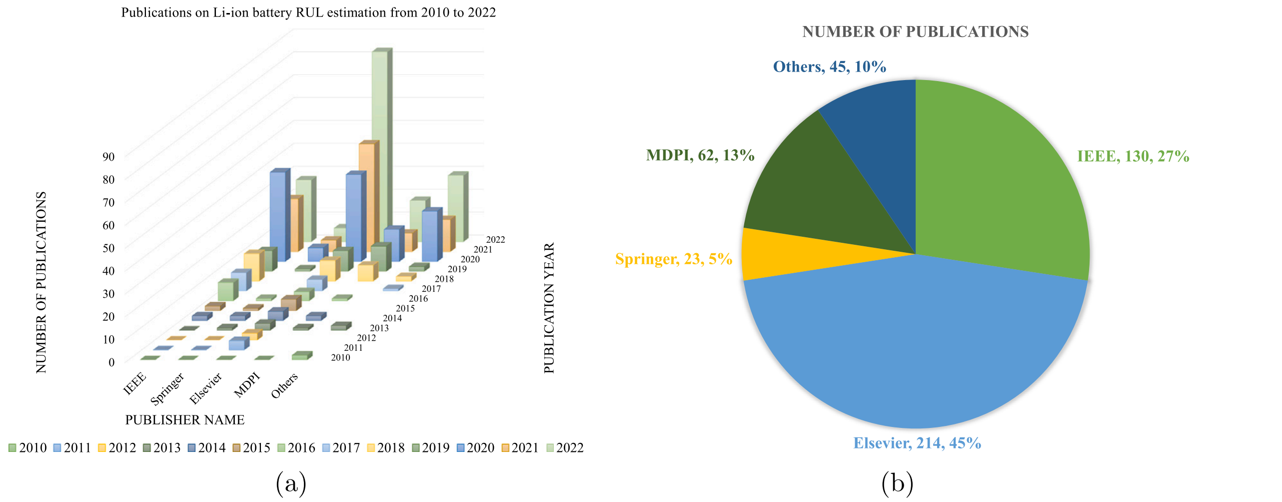

Fig. 2. (a) Evolution of Li-ion battery remaining useful life prediction research: 3D column chart depicting publication trends from 2010 to 2022. (b) Analysis of publications on RUL of lithium-ion battery in prominent journals from 2010 to 2022.

are then applied to predict the RUL and estimate battery degradation [12]. However, a major challenge with data-driven methods is the requirement for a large amount of historical data to train the models.

RUL prediction approaches that are based on mathematical models have also garnered considerable interest among researchers. These models can be categorized into empirical models [13] and the physics of failure models [14]. The physics of failure models are developed based on an understanding of battery material properties, loading scenarios, and failure mechanisms. However, constructing the physics of failure models is challenging due to the need for specialized equipment and conducting complex electrochemical tests to determine model parameters [15]. Consequently, their acceptance for onboard applications is limited. For this data, data-driven approaches are considerably more convenient, and deep learning-based approaches are gaining the interest of researchers. In a recent publication [16], the author proposed a hybrid approach for RUL prediction, combining an adaptive Levy Flight Optimized PF with a Long Short-Term Memory (LSTM) network.

Enhancement of battery voltage models is necessary to improve speed, handling of discontinuities, generalization to real-world conditions, robustness across battery types, and accuracy [17]. To improve LSTM battery voltage models, two novel techniques were presented in [18]: sequence training and data shuffling. These techniques resulted in a significant 22% reduction in voltage estimation error (from 28.5 mV to 22.3 mV RMS error) across various conditions (−20 °C to 25 °C). The study's shortcomings, however, may lie in its primary voltage prediction focus, which may have obscured other aspects of battery behavior and possible differences in efficacy across various battery chemistries and operating conditions. In [19], a unique PF framework incorporating a gray neural network (GNN) for RUL prediction of LIBs was introduced. The utilization of CNNs in the prediction of RUL can handle the dynamic degradation and nonlinear characteristics exhibited by LIBs. To better understand battery thermal management in electric vehicles, Ref. [20] looks into how temperature and depth of discharge (DoD) affect heat generation in Li-ion batteries. However, the emphasis on a single battery type and the requirement for additional validation across various battery chemistries and configurations are drawbacks.

Lithium iron phosphate (LFP) and lithium nickel cobalt aluminum oxide (NCA) cells are pivotal in predicting the RUL of LIBs due to their distinct electrochemical characteristics [21]. Due to strong hysteresis effects, the first order resistor capacitor (1RC) with hysteresis model performed best for LFP and NCA cells, according to [22], although all three equivalent circuit models (ECMs) showed low errors in battery voltage prediction across tested lithium-ion battery chemistries. The study's focus on a small number of chemicals and conditions is one of its limitations, though, as it may limit the applicability of its conclusions to more diverse contexts and applications.

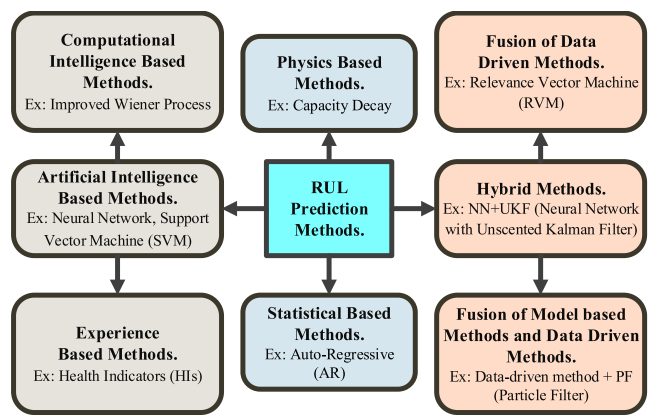

Fig. 3. A summary on different RUL prediction methods.

Effective cooling of Li-ion batteries is crucial for extending their lifespan and predicting RUL accurately [23]. Considering this, the performance of a magnetohydrodynamic (MHD) pump-based microchannel cooling system is examined in [24]. It is found that while efficiency decreases, applied voltage and Hartmann number increase velocity, heat removal rate, and Nusselt number. In terms of heat transfer performance, Cu–water nanofluid performs better than TiO_2-water and Al_2O_3-water nanofluid. A thorough understanding of the MHD pump's suitability in various cooling scenarios could be obtained by investigating the thermal performance under different conditions, such as fluid flow rate and channel geometry, which is not done in this study.

Fig. 3 provides a visualization of various categories of RUL prediction techniques. There are classical statistical methods and physics-based methods to predict the RUL of LIBs, as well as modern AI, DL, and hybrid methods. These techniques encompass the use of CNNs, particle filtering, and hybrid approaches to handle the complex nature of RUL prediction for LIBs. Applications of ANN, SVM, LSTM, and GNN are examples of artificial intelligence-based methods for RUL prediction of LIBs. Additionally, computational intelligence-based methods such as improving the Wiener process, and experience-based methods such as health indicators are also prominent for RUL prediction of LIBs. However, hybrid methods such as NN with UKF are gaining more popularity among researchers.

Optimization techniques are important in deep learning for improving training efficiency, updating parameters, avoiding local minima, regularization, and hyperparameter tuning. A meta-heuristic algorithm named bat algorithm inspired by bats is presented by Yang [25]. The bat algorithm demonstrates superior adaptive ability and convergence precision compared to traditional particle swarm optimization algorithms. Combining the bat algorithm with intelligent PF holds great potential for the future of PF technology. Wu et al. [26] hypothesized in 2019 that a combination of neural networks (NN) and bat-based PF could be utilized for RUL prediction of LIBs. Similarly, Lian et al. [27] described an RUL prediction approach for LIBs using bat-based PF with a semi-empirical model. However, those methods require additional feature extraction from the data sets to predict the RUL properly, which may require complex calculation and preprocessing. In our proposed methodology, we have used the CNN architecture to predict the RUL of the LIBs, and it has given us a way of extracting features automatically, which also saves additional calculation steps for manual feature extracting and permits us to predict the RUL conveniently. Furthermore, the proposed methodology also allows us to achieve a greater result in predicting the RUL in a shorter period. As mentioned earlier, the traditional RUL techniques may not be sufficient to get a satisfactory result in predicting the RUL because of their data handling capabilities and computational power limits. The proposed methodology not only gives an upper hand in predicting the RUL of LIBS by proving a significant result but also its adaptability to various battery models.

In this paper, we propose a novel approach for intelligent battery RUL prediction by combining bat-based optimization and a Convolutional Neural Network (CNN) model. Our method improves the accuracy of existing particle filter (PF)-based RUL prediction techniques in two key ways.

- Firstly, we introduce a CNN architecture specifically designed for capacity degradation modeling. Unlike traditional empirical models, the CNN architecture offers enhanced precision in capturing diverse degradation trends. This enables more accurate RUL prediction, thereby improving the overall prediction performance.
- Secondly, we employ the Bat-optimization technique to update the weights and biases of the CNN architecture. Inspired by the movement patterns of bats, this optimization technique guides the particles towards areas of higher probability based on updated capacity information. As a result, the Bat-optimization technique improves the particle distribution in a robust manner, leading to enhanced prediction accuracy even in challenging scenarios.

The rest of the paper is organized as follows: Section "Dataset" describes the dataset that has been used in this research with the proposed CNN capacity degradation model. Section "Methodology" discusses the methodology of this research and the Bat-optimization theory with the recommended approach for RUL prediction. Experimental results are analyzed and compared with other prediction methods in Section "Results". Further analysis of the results and the relevant discussion is given in Section "Discussions". Finally, the paper is concluded in Section "Conclusion" with some future remarks.

Dataset

RUL prediction of LIBs relies on two critical factors: the battery's cycle count and its known capacity. As the battery undergoes successive charging and discharging cycles, its capacity gradually decreases. Impedance tests provide insights into the internal properties of the battery that change as it degrades, while frequent cycling accelerates battery aging. In this study, we utilize a CNN model to elucidate the mechanism behind battery capacity degradation, specifically how batteries gradually lose their supply of lithium ions. Fig. 4 illustrates the capacity degradation of different battery models at various ambient temperatures, highlighting the significant impact of temperature on capacity degradation and battery lifecycle. Capacity degradation is rapid in higher ambient temperatures (43 °C) compared with low ambient temperatures (4 °C). Consequently, it can be inferred that discharging batteries at elevated temperatures accelerates the degradation of battery life. C-rate, denoted as C, is a measurement of the charge and discharge current concerning the nominal capacity of a battery. It is commonly used in battery technology to express the rate at which a battery is charged or discharged relative to its capacity. For example, a C-rate of 1C indicates that the current is equal to the nominal capacity of the battery. In contrast, a C-rate of 0.5C implies that the current is half of the nominal capacity.

The technical specifications of the battery cell used in this work are as follows:

- Nominal voltage: Around 3.7 V for LIBs.
- Nominal capacity: For the $LiCoO_2$ commercial battery, it is approximately 2 Ah.
- Anode material: Lithium Cobalt Oxide ($LiCoO_2$)
- Cathode material: Graphite.
- Electrolyte material: Lithium hexafluorophosphate ($LiPF_2$) dissolved in a mixture of ethylene carbonate (EC) and dimethyl carbonate (DMC).

The dataset utilized in this study is collected from the Prognostics Center of Excellence (PCoE), a division of NASA that specializes in prognostic research. The dataset comprises experimental data obtained from the LIBs, specifically the 18,650 $LiCoO_2$ commercial battery [28]. From the available LIB experimental data, a careful selection process was conducted to choose specific batteries for testing the proposed algorithm. Battery005, Battery006, Battery007, Battery018, Battery029, Battery030, Battery031, Battery041, and Battery055 were chosen based on a preliminary analysis of their cell capacity degradation data and experimental conditions [29]. The threshold capacity for defining the end-of-life point was set at 1.4 Ah, considering that each of the selected cells has a nominal rated capacity of 2 Ah (with a slightly varied discharge cycle). The capacity failure criteria were established at 70% of the original rated capacity. These choices were made to ensure consistency across the experiments and enable effective evaluation of the proposed algorithm. The dataset possesses various characteristics and encompasses the following experimental conditions [29]:

- The impedance is documented in the data set as a degradation indicator with charging–discharging at various temperatures.
- The dataset is provided in MATLAB file format as a sophisticated 3D array.
- Run the charge, discharge, and impedance operating profiles three times at room temperature.
- Until the cell potential reached 4.2 V, charging was conducted at 1.5 A in a constant current (CC) mode. Afterward, the charge current was held in a constant voltage (CV) mode until it reached 20 mA. Cells 5, 6, 7, and 18 were discharged at a constant current (CC) level of 2 A until their potentials reached 2.7 V, 2.5 V, 2.2 V, and 2.5 V, respectively.
- Electrochemical impedance spectroscopy (EIS) was applied to assess impedance using a frequency change from 0.1 Hz to 5 kHz.
- Impedance tests give insight into the internal battery properties that alter as aging occurs, while recurrent charge and discharge cycles accelerate the aging of the batteries. When the batteries met the end-of-life (EOL) threshold, which was a 30% decline in rated capacity, the tests were terminated (starting at 2 Ahr to 1.4 Ahr).

The feature co-relation matrix of the LIB data set is shown in Fig. 5 and from the co-relation score, we can see some of the features are highly correlated, such as capacity, the temperature measured, voltage load, the voltage measured, and others that can be seen from the correlation score. The correlation values can vary from −1 to 1. In general, 1 means a strong correlation, 0 means neutral, and −1 indicates a correlation that may not be strong enough.

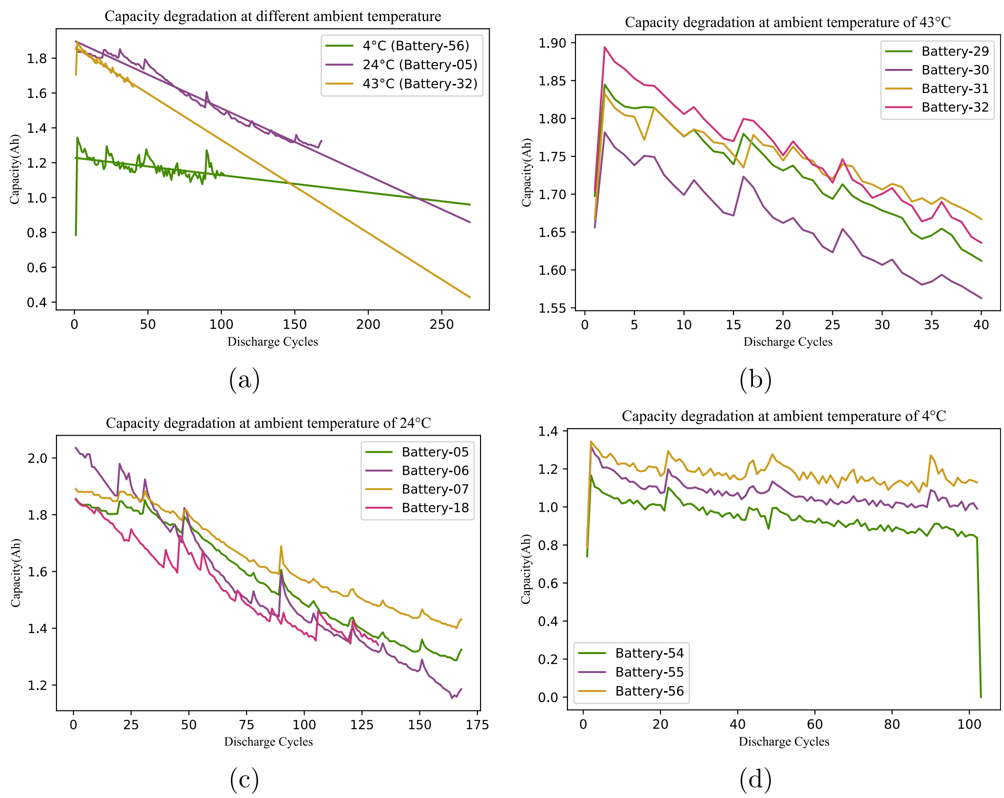

Fig. 4. (a) The slope of the capacity degradation rises when the temperature increases; (b), (c), and (d) the visual plot of the capacity degradation of batteries in various ambient temperatures.

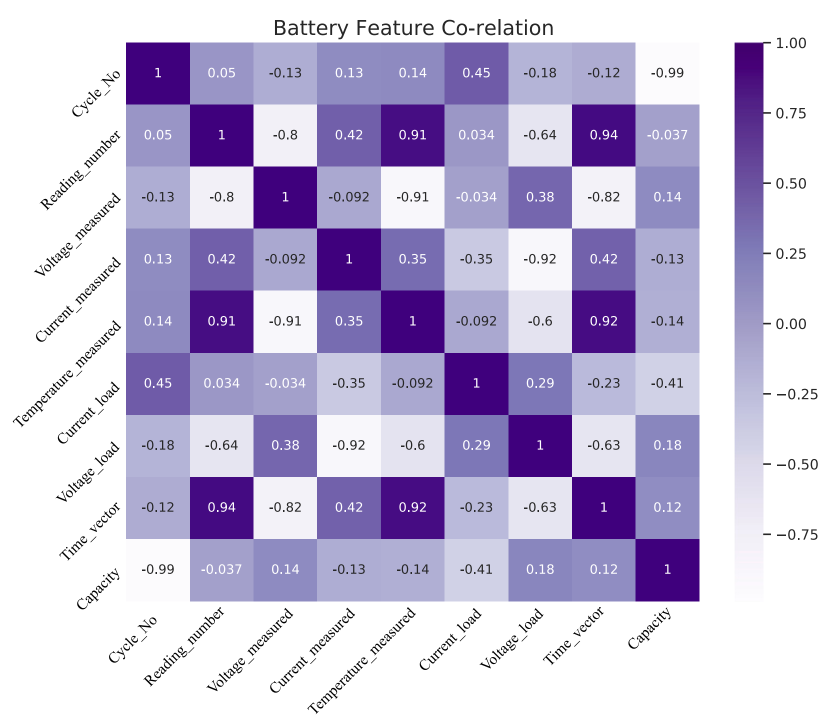

Fig. 5. A co-relation matrix among all the data features of LIB.

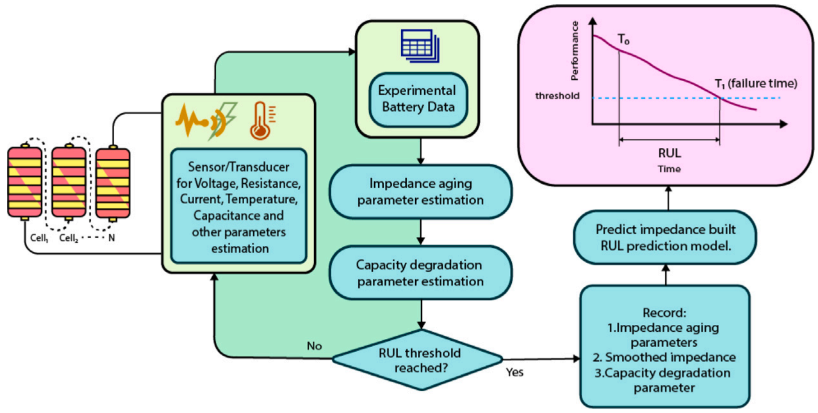

Fig. 6. Data generation to RUL prediction procedure of LIBs for proposed RUL prediction algorithm.

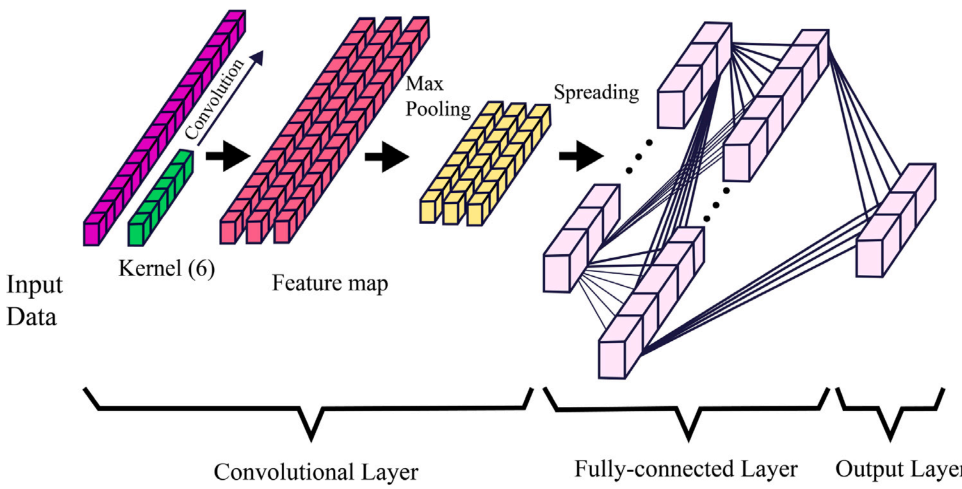

Fig. 7. 1D CNN architecture employing a 1D kernel.

Methodology

CNN degradation model

In this study, we employ a CNN architecture to simulate battery degradation under various operating conditions. The proposed approach involves integrating a bat-inspired particle filter to iteratively update the parameters of the CNN model. By leveraging the bat algorithm, the particle distribution is optimized, effectively guiding the particles toward high-likelihood regions. Conventionally, a CNN consists of three layers: convolutional, pooling, and fully connected layer. Fig. 6 explains the RUL prediction process, starting from data acquisition to RUL prediction for LIBs. Here, experimental battery data is collected through sensors or transducers, and this data is utilized for capacity degradation analysis, followed by the RUL prediction process. Fig. 7 illustrates the architecture of the 1D-CNN algorithm, where the input layers are transformed into a 1D convolutional layer, and after pooling and convolution steps, a fully connected layer is created to ultimately generate the output layer.

CNNs are a specialized type of Deep Neural Network commonly employed for analyzing visual data by automatically extracting high-level features [30]. However, the applicability of CNNs has expanded, and they are now extensively used for regression and classification tasks involving time-series tabular data. Three types of CNNs are found in the literature: 3D CNNs, 2D CNNs, and 1D CNNs. In the domain of natural language processing and sequence modeling, 1D CNNs are commonly utilized. This is particularly relevant for battery capacity data, which is represented as a one-dimensional time series analysis, necessitating the use of 1D CNNs. The following equations demonstrate the activation function calculation and the convolution operation applied to the input data (a 1D vector) within the one-dimensional convolutional layer [31]. Fig. 8 gives an illustration of the CNN architecture used in this research. The inputs are “Cycle No”, “Voltage measured”, “Current measured”, “Temperature measured”, “Current load”, “Voltage load”, and “Time vector”. The model’s output is “Capacity” for RUL prediction. The model architecture consists of a convolutional neural network (CNN), and dense layers. The first convolutional layer uses the ReLU activation function and 256 filters with a kernel size of 6, padding the input to preserve its shape. The data is then reshaped using a flattening layer and a max-pooling layer with a pool size of 1. The next seven dense layers are fully connected and have ReLU activation. They contain 256, 128, 64, 32, 16, 8, and 4 neurons in each layer, respectively. Without an activation function specified, the output layer of the model consists of a single neuron that represents the regression output, allowing the model to predict continuous output values.

$$\mathrm{x}_{\iota}^{l} = \sum_{i=1}^{N_{l-1}} conv1D(\mathrm{w}_{i\iota}^{l-1}, \mathrm{s}_{i}^{l-1}) + \mathrm{b}_{\iota}^{l} \tag{1}$$

where, x_{ι}^{l} represents the input given to layer l for the ιth neuron, b_{ι}^{l} is the bias of the ιth neuron in layer l, $w_{i\iota}^{l-1}$ symbolizes the convolution kernel connecting the ith neural node in layer $l-1$ to the ιth neural node in layer l, s_{i}^{l-1} stands for the output of the ith neural node in layer $l-1$, N_{l-1} indicates the number of neural nodes in layer $l-1$, and the conv1D refers to the one-dimensional convolution operation. The output of a neural node after applying an activation function is given

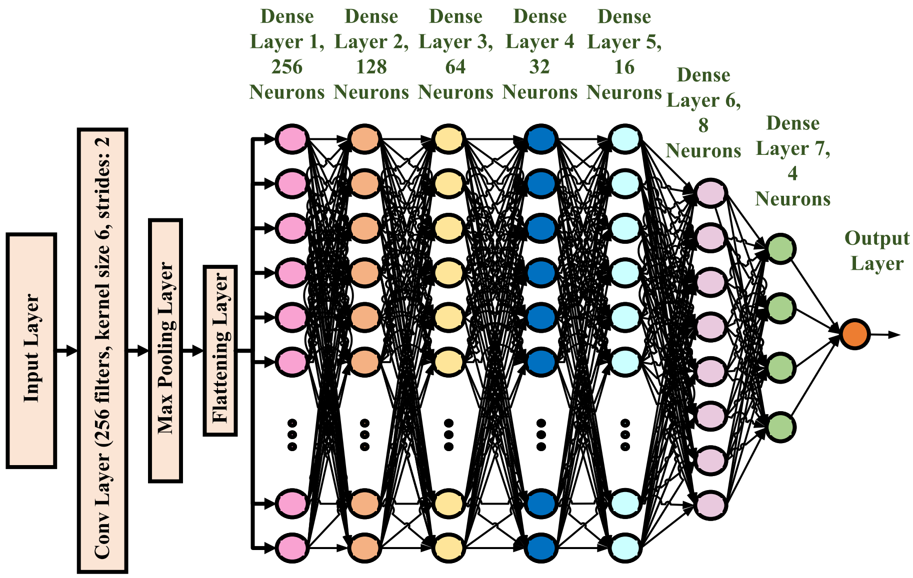

Fig. 8. CNN architecture used in this research to predict the LIBs RUL.

by (2).

$$s_t^l = f(x_t^l) \tag{2}$$

Here, we proposed and assessed the accuracy of the degradation model. However, for accurate RUL prediction, it is crucial to update the model parameters at each cycle. One effective approach to address the parameter adjustment is through the use of PF and other related methods. In the following section, we introduce an enhanced optimization technique for PF, known as the Bat-optimization algorithm. This meta-heuristic algorithm improves the parameter adjustment process in PF, leading to more accurate RUL prediction. Furthermore, we provide a detailed description of our RUL prediction method that relies on the Bat-optimization algorithm. We explain how the Bat-optimization algorithm enhances the performance of PF, enabling us to achieve more reliable and precise RUL prediction.

The boundary conditions that were taken into account during the model development process are as follows:

- Operating Temperature Range: The battery degradation data used for model development were collected and analyzed within an operating temperature range of 24 °C. This temperature range corresponds to the ambient conditions for battery models B0005, B0006, B0007, and B0018, ensuring consistency and relevance in the data analysis.
- The voltage limits considered in the model were set at 3.7 V, reflecting the typical operating voltage range for Lithium-ion Batteries.
- The capacity failure criteria were established at 1.4 Ah, corresponding to 70% of the original rated capacity. This threshold value serves as a critical boundary condition for determining the end of the battery's useful life.
- Constant current: During the data collection process, a constant current of 2 A was applied to the batteries to simulate realistic operating conditions.
- EIS Frequency Range: EIS data were collected over a frequency range of 0.1 Hz to 5 kHz. This frequency range ensures a comprehensive characterization of the battery's electrochemical behavior.

Bat-optimizer

The Bat optimization is based on a meta-heuristic algorithm, namely the Bat algorithm. Certain multimodal and complex problem types are challenging for traditional methods to handle [32]. When aiming to achieve optimal or suboptimal solutions in intricate multimodal scenarios, a nature-inspired population-based algorithm named the Bat algorithm (BA) can be useful due to its stochastic-based variation and intensification abilities [25,33]. The BA draws inspiration from the echolocation and bio-sonar traits of microbats [34], using them as a guide for their hunting techniques. Bats use echolocation to identify potential prey, navigate their surroundings, and return to their roosts while flying through dense vegetation. When a bat employs echolocation, it constructs a three-dimensional representation of its environment using sound pulses. Bats emit stronger pulses at a lower frequency to scan for prey, and when they detect prey, they emit softer pulses at a higher frequency.

Overview of Bat Algorithm

Echolocation is a technique widely used by many bat species. It involves emitting sound pulses to navigate and locate prey in the dark. Microbats emit high-frequency sound pulses and listen for echoes reflected from nearby objects [35]. They can produce 10 to 20 sound bursts per second, which increases to 200 pulses per second when they are hunting. The ultrasonic frequencies used by microbats typically range from 25 kHz to 150 kHz due to the speed of sound in air, which is approximately $v = 340$ m/s. This results in wavelengths (λ) ranging from 2 mm to 14 mm, with a constant frequency f, given by $\lambda = \frac{v}{f}$. Interestingly, these wavelengths are similar in size to those of their prey. We can relate aspects of echolocation to the objective function of an optimization method, leading to the Bat Algorithm [25]. Fig. 9 gives an illustration of the Bat algorithm, specifying every step and operation.

The Bat Algorithm incorporates key features of echolocation to enhance the optimization process. For clarity, we focus on certain aspects of echolocation and formulate the following three idealized rules:

1. Bats use echolocation to measure distance and distinguish between food/prey and background obstacles.
2. Bats fly randomly with velocity v_i at position x_i, utilizing a frequency f_{min}, variable wavelength λ, and loudness A_i to search for prey. Depending on their proximity to the target, they can adjust both the wavelength (or frequency) and the rate of pulse emission (r) in the range of [0, 1].
3. Loudness can vary widely, but for our purposes, we assume it ranges from a large positive value A_i to a minimum constant value A_{min}.

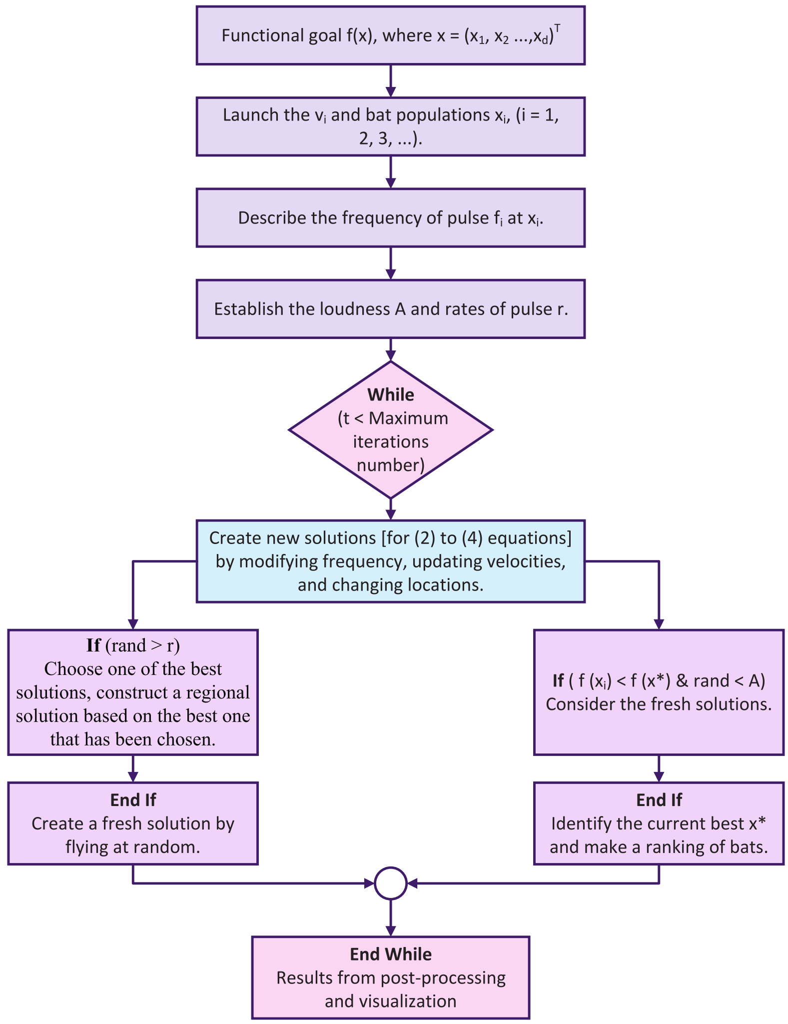

Fig. 9. A flow diagram of the Bat algorithm describing all the necessary operations.

Although ray tracing is a computationally intensive technique that could enhance the algorithm, we exclude it here for simplicity. The choice between frequency and wavelength depends on the problem context [36].

Bat motion

At each iteration n, we record the positions x_i^n and velocities v_i^n of all bats in the search space. We denote the currently optimal bat solution as x^*. The three rules mentioned above can be expressed as equations for the rate of change of x_i^n and velocities v_i^n:

$$f_i = f_{min} + \left(f_{max} - f_{min}\right)\eta \tag{3}$$

$$v_i(n) = v_i(n-1) + \left(x_i(n-1) - x^*\right) f_i \tag{4}$$

$$x_\kappa^i(n) = x_\kappa^i(n-1) + v_i(n) \tag{5}$$

Here, $\eta \in [0, 1]$ is an arbitrary scalar with a uniform distribution. $x_\kappa^i(n)$ represents the position of bat i along the κ-th dimension in the search space at iteration n. $v_i(n)$ represents the velocity of bat i at iteration n, which influences how the position of the bat changes in the κ-th dimension.

We can implement either wavelengths or frequencies, depending on the context. For instance, with $f_{min} = 0$ and $f_{max} = 100$, the choice of frequency range depends on the problem's domain size. Initially, each bat is assigned a random frequency from $[f_{min}, f_{max}]$. Thus, the bat algorithm can be seen as a frequency-tuning technique that balances exploration and exploitation. Local search involves small random changes around the current optimal solution, as described by:

$$x_{\text{new}} = x_{\text{old}} + \varepsilon A(n) \tag{6}$$

Here, the random number ϵ is drawn from $[-1, 1]$, while $A(n)$ is the average loudness of all the bats at the current time step. This equation forms the primary update mechanism in the optimization algorithm.

Loudness and pulse rate variations

To regulate exploration and exploitation effectively, it is essential to adjust loudness A_i and pulse emission rate r_i during iterations. Loudness typically decreases when a bat finds prey, while the pulse emission rate increases. Loudness can be set to any value between A_{min} and A_{max}, with A_{min}= 0 representing the moment when a bat has found prey and temporarily stops emitting sound. With these assumptions, we describe:

$$A_i(n+1) = \alpha A_i(n) \qquad (0 < \alpha < 1) \tag{7}$$

$$r_i(n+1) = r_i(0)[1 - \exp(-\gamma n)] \qquad (\gamma > 0) \tag{8}$$

Here, α and γ are constants, with α being analogous to the cooling factor in simulated annealing. Given the conditions $0 < \alpha < 1$ and $\gamma > 0$, we can conclude that:

$$\mathrm{A}_i(n) \to 0, \mathrm{r}_i(n) \to \mathrm{r}_i(0), \text{ as } n \to \infty \tag{9}$$

RUL prediction

The RUL of LIBs can be predicted in real-time by combining the bat optimization algorithm and the CNN degradation model. A state-space model based on the CNN degradation model is constructed using historical battery capacity degradation data, and the states are fine-tuned using the bat optimization algorithm. To determine the RUL, the updated degradation model is then projected to the failing threshold. The process is described in detail below.

Construction of the state-space model

The biases and weights of the two-neuron CNN models are designated as the system states, *i.e.*, [IW1, IW2, b11, b12, LW1, LW2, b2], where biases are b11, b12, b2 and weights are IW1, IW2, LW1, LW2. It is presumed that the random walk mode applies to these seven states. It is important to note that the cell capacity is the actual vector being measured. This allows us to design the following state-space model. The details of this model can be found in [26].

$$\theta_\kappa = \begin{bmatrix} \mathrm{IW}_{1,\kappa} \\ \mathrm{IW}_{2,\kappa} \\ b_{11,\kappa} \\ b_{12,\kappa} \\ \mathrm{LW}_{1,\kappa} \\ \mathrm{LW}_{2,\kappa} \\ b_{2,\kappa} \end{bmatrix} = \begin{bmatrix} \mathrm{IW}_{1,\kappa-1} \\ \mathrm{IW}_{2,\kappa-1} \\ b_{11,\kappa-1} \\ b_{12,\kappa-1} \\ \mathrm{LW}_{1,\kappa-1} \\ \mathrm{LW}_{2,\kappa-1} \\ b_{2,\kappa-1} \end{bmatrix} + \begin{bmatrix} w_1 \\ w_2 \\ w_3 \\ w_4 \\ w_5 \\ w_6 \\ w_7 \end{bmatrix}, \quad \begin{matrix} w_1 \sim \mathcal{N}(0,\sigma_1^2) \\ w_2 \sim \mathcal{N}(0,\sigma_2^2) \\ w_3 \sim \mathcal{N}(0,\sigma_3^2) \\ w_4 \sim \mathcal{N}(0,\sigma_4^2) \\ w_5 \sim \mathcal{N}(0,\sigma_5^2) \\ w_6 \sim \mathcal{N}(0,\sigma_6^2) \\ w_7 \sim \mathcal{N}(0,\sigma_7^2) \end{matrix} \tag{10}$$

$$Q'_\kappa = \mathrm{CNN}(\theta_\kappa, \kappa) + \upsilon, \quad \upsilon \sim \mathcal{N}(0, \sigma_\upsilon^2) \tag{11}$$

where θ_κ represents a parameter vector, and $\theta_{\kappa-1}$ represents the previous parameter vector. The variables w_1 through w_7 are random variables following Gaussian distributions with variances σ_1^2 through σ_7^2, respectively. Q'_κ is the result of the CNN degradation model with parameters θ_κ and iteration κ, and υ represents Gaussian noise.

The working procedure for the proposed RUL prediction approach is shown in Fig. 10. The process starts with the collection of battery degradation data and then processing the data for CNN. After the construction of the degradation model, the bat-based particle filter is used for better particle distribution, and later, the state space model is updated to calculate the battery capacity for predicting the RUL. Python was used to create the state space model for this study, taking advantage of its strong numerical computation and modeling capabilities. Python made it easier to build a versatile and adaptable model for assessing the system's dynamics and forecasting future states from the available data.

Updating the states depending on Bat PF

The database containing previous batteries with identical specifications to the test battery is employed to acquire prior state information for the PF algorithm. By using historical sample data to train the deterioration model, the CNN model parameters are initialized. The parameters can then be adjusted depending on the test battery's available capacity data by employing the state-space model and bat optimization. Upon obtaining the posterior distribution of the model variables $\{\theta^i_\kappa, \omega^i_\kappa\}_{i=1}^n$, the capacity at κ can be predicted as:

$$Q_\kappa = \sum_{i=1}^n \omega^i_\kappa Q^i_\kappa = \sum_{i=1}^n \omega^i_\kappa \mathrm{CNN}\left(\theta^i_\kappa, C_\kappa\right) \tag{12}$$

By projecting out the CNN degradation model, the capacity at $\kappa + l$ can be estimated as:

$$Q_{\kappa+l} = \sum_{i=1}^n \omega^i_\kappa Q^i_{\kappa+l} = \sum_{i=1}^n \omega^i_\kappa \mathrm{CNN}\left(\theta^i_\kappa, C_{\kappa+l}\right) \tag{13}$$

As such, the RUL of the i-th particle at κ, (RUL^i_κ) can be predicted in line with:

$$\mathrm{CNN}\left(\theta^i_\kappa, C_\kappa + \mathrm{RUL}^i_\kappa\right) = threshold \tag{14}$$

Table 3
Experiment results of various models with same data.

Model	RMSE (Ah)	MAE (Ah)	R2
Linear Regression	0.04321	0.04254	0.69
SVR	0.03429	0.02828	0.85
Ridge	0.04037	0.03625	0.65
ANN	0.02061	0.01937	0.93

Approximating the RUL's posterior pdf at κ can be done with the following formulas:

$$p\left(\mathrm{RUL}_\kappa | Q_{1:\kappa}\right) \approx \sum_{i=1}^n \omega^i_\kappa \delta\left(\mathrm{RUL}_\kappa - \mathrm{RUL}^i_\kappa\right) \tag{15}$$

$\delta(.)$ is the Dirac delta function, which is used to model an impulse or spike at a specific point. In this context, it acts as an impulse function.

An prediction of RUL can be obtained by:

$$\mathrm{RUL}_\kappa = \sum_{i=1}^n \omega^i_\kappa \mathrm{RUL}^i_\kappa \tag{16}$$

Results

The developed RUL prediction algorithm has undergone rigorous testing to evaluate its accuracy and robustness, utilizing NASA datasets. Additionally, a comparative analysis is conducted by combining the CNN model with bat optimization (CNN+bat optimization) to further assess its superiority. The effectiveness of the proposed strategy is evaluated based on three key metrics: root mean square error (RMSE), R2 score (coefficient of determination), and mean absolute error (MAE). Various performance metrics are commonly employed to evaluate the CNN model, including mean squared error (MSE), root mean squared error (RMSE), R2 score, and MAE. Lower values of MSE, RMSE, and MAE indicate better performance, whereas a higher R2 score indicates a stronger ability to predict outcomes. The prediction accuracy is enhanced when RMSE and MAE approach zero, while an R2 score value close to 1 signifies a more accurate prediction outcome. The expressions of performance metrics are as follows:

$$RMSE = \sqrt{\frac{1}{n}\sum_{k=1}^n (y_k - \hat{y}_k)^2} \tag{17}$$

$$MAE = \frac{1}{n}\sum_{k=1}^n \left|\frac{(\hat{y}_k - y_k)}{y_k}\right| \tag{18}$$

$$R^2 = 1 - \frac{\sum_{k=1}^n (y_k - \hat{y}_k)^2}{\sum_{k=1}^n (y_k - \bar{y}_k)^2} \tag{19}$$

Here y_k denotes the rated battery capacity, $\hat{y}_k$ represents the prediction of battery capacity, and $\bar{y}_k$ is the mean or average value of the rated battery capacity y. In this paper, the proposed model resulted in an RMSE of 0.00656015, an MAE of 0.00439, and an R2 value of 0.998712 for the full dataset of the B005 battery model. The result is better when compared to other methods that use PFs and is far better than conventional prediction methods.

Experiments were conducted using NASA's dataset, where various machine-learning models were initially implemented on the same data, and their results were observed. Table 3 illustrates various experimental results. Among these models, the Artificial Neural Network (ANN) yielded the best performance, achieving an RMSE value of 0.02061, an MAE of 0.0197, and an R2 score of 0.93. However, the proposed model introduced in this research surpasses the performance of all implemented models.

There were a total of 11 battery model data sets available in the datasets. The capacity prediction illustration can be found in Fig. 12 for the batteries that have remaining useful cycles left under the failure threshold capacity of 1.44 (Ah). From Fig. 4, it is noted that except for the battery models B0005, B0006, B0007, and B0018, which are

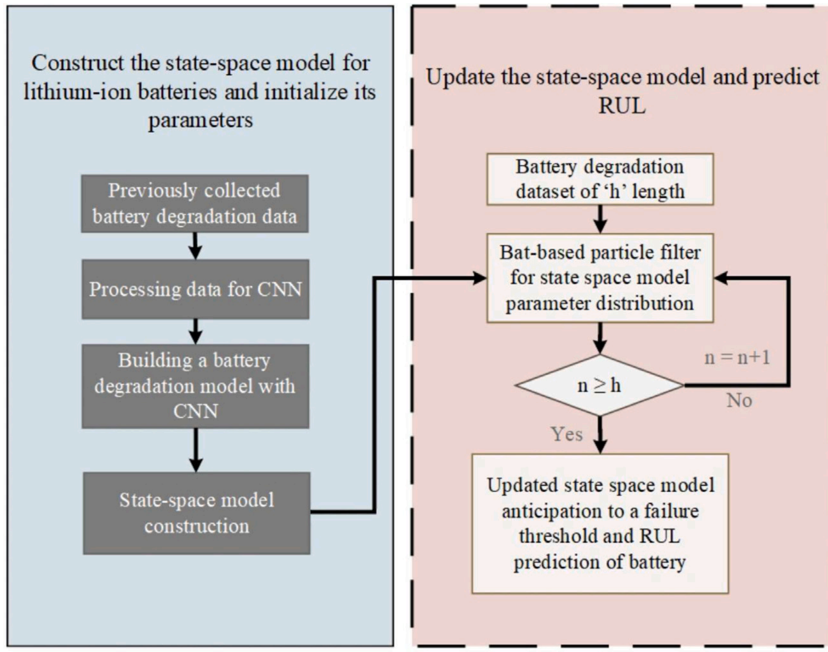

Fig. 10. Working procedure of the proposed RUL prediction model based on CNN and Bat-based optimizer.

Table 4
Prediction result of battery B0005, B0006, B0007, and B0018.

Battery model	RMSE (Ah)	R2 Score	MAE (Ah)
B0005	0.00656015	0.998712	0.004397067
B0006	0.00884308	0.998572	0.005815670
B0007	0.00635205	0.998279	0.00428309
B0018	0.00810393	0.997305	0.005490191

Table 5
Simulation results using different optimizers.

Optimizer	MSE Ah	RMSE Ah
Bat	0.000043035	0.0065601
Adam	0.0015	0.0387298
RMSProp	0.0030	0.054772
SGD	0.0042	0.064807
Adagrad	0.0066	0.0812403
Adadelta	0.6605	0.8127

in the ambient temperature of 24 °C, the other batteries have already reached the failure threshold or do not have data in the range of 1.44 (Ah) capacity threshold. Therefore, they do not have any RUL available. Table 4 illustrates the LIBs RUL prediction results with a complete evaluation of the proposed method.

Fig. 12 shows various battery model capacity prediction graphs with CNN and bat optimizer. The vertical axis and horizontal axis represent the capacity and the number of cycles, respectively. In the figures, we can see that the expected and predicted graphs are close but not overlapping each other. In Fig. 13, the RUL of the batteries that stay within the range of the failure threshold is illustrated. Battery B0005 is almost at its end of life, having only 2 actual remaining charge or discharge cycles above the failure threshold of 1.44 (Ah) capacity, and the predicted number of remaining cycles is 3. Battery B0006 and B0018 also have a low number of remaining useful life. The battery model B0007 has almost 31 cycles of remaining useful life in actual and predicted results. Table 5 provides a comparison of various optimizer results, where the Bat optimizer gives the lowest MSE of 0.000043035 Ah and RMSE of 0.0065601 Ah for the anticipated battery models.

In Table 9, the results of different RUL prediction models utilizing CNN architecture are presented. A comparison between the findings of Tables 4 and 9 reveals that our proposed model surpasses all others in performance.

Discussions

Table 6 carries the comparison of various RUL prediction methods results using PFs, while Table 8 shows the comparison of different deep learning algorithms of RUL prediction. For the dataset provided by the NASA PCoE, the proposed method is capable of giving a lower RMSE value of 0.00656 in comparison to SGM-LORPF [37]. From Table 6, it is noted that the Semiempirical model with Bat-PF [27] provides a lower RMSE value for different datasets provided by the CALCE battery research group. However, the lack of transferability of this method limits its application to novel or untested compounds, as the dataset by CALCE consisted of tested compounds only. Fig. 11(a) shows the learning curve of the mode. It can be seen that the model earns stability in around 819 epochs. The figure indicates that the model is learning the training data properly and the model is not overfitting. Fig. 11(b) illustrates the error histogram that shows the difference between the actual and predicted output.

Based on the results presented in Table 8, the proposed model, which utilizes CNN and is fine-tuned with the Bat optimizer, demonstrated the most accurate performance in predicting the RUL of LIBs, with the lowest RMSE recorded at 0.656%. The obtained result confirms that the proposed model serves as a valuable tool to achieve methodological balance, effectively mitigating issues related to overfitting and underfitting. After thorough analysis, it is evident that the model developed in this study achieved a state of perfect equilibrium, characterized by the optimal selection of activation functions, learning rates, optimizers, and other pertinent variables.

The precise result in the training data ensures that the proposed model is not underfitted. From the validation metrics, including loss, RMSE, and R2 score, it can be seen that the model has not overfitted either. Both L1 and L2 regularization techniques are implemented in the

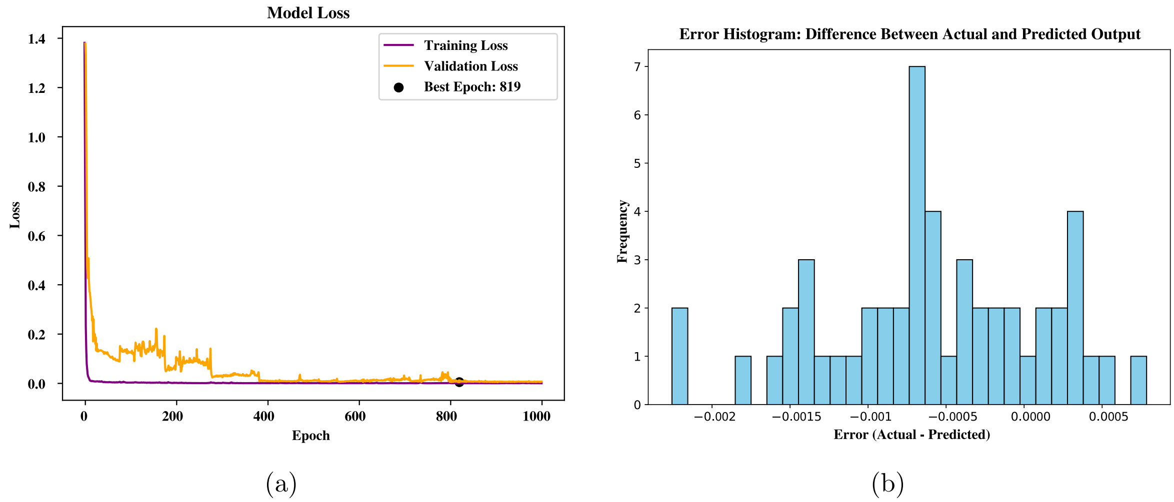

Fig. 11. (a) CNN model learning curve with best epoch.(b) Error Histogram Plot.

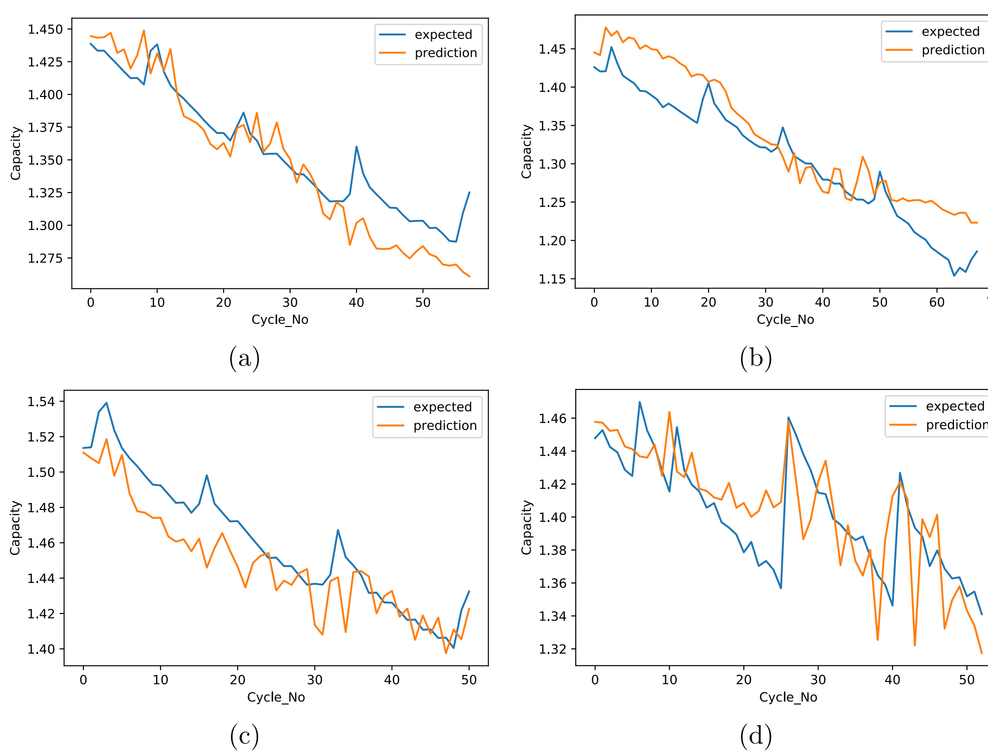

Fig. 12. Capacity prediction of different battery models: (a) Battery model B0005, (b) Battery model B0006, (c) Battery model B0007, (d) Battery model B0018.

Table 6
Comparison of various methods for estimating remaining useful life using particle filters.

Method	Dataset/ Battery model	Test condition	Result	Publication year	Ref.
Exponential model + PF	NASA PCoE B005	Starting cycle is 100	Absolute error 8	2018	[38]
NN + Bat-PF	NASA PCoE RW11	100.02 prediction days	Absolute error 2.19	2019	[26]
Semi-empirical model + Bat-PF	CALCE	–	RMSE 0.00024 and Absolute error 15	2020	[27]
SGM-LORPF	NASA PCoE B0005	Starting cycle is 2/3 of whole life cycle	RMSE 0.0229 and Absolute error 5	2020	[37]
CNN + Bat optimization	NASA PCoE B0005	167 cycles	RMSE 0.00656 and MAE 0.0043	–	–

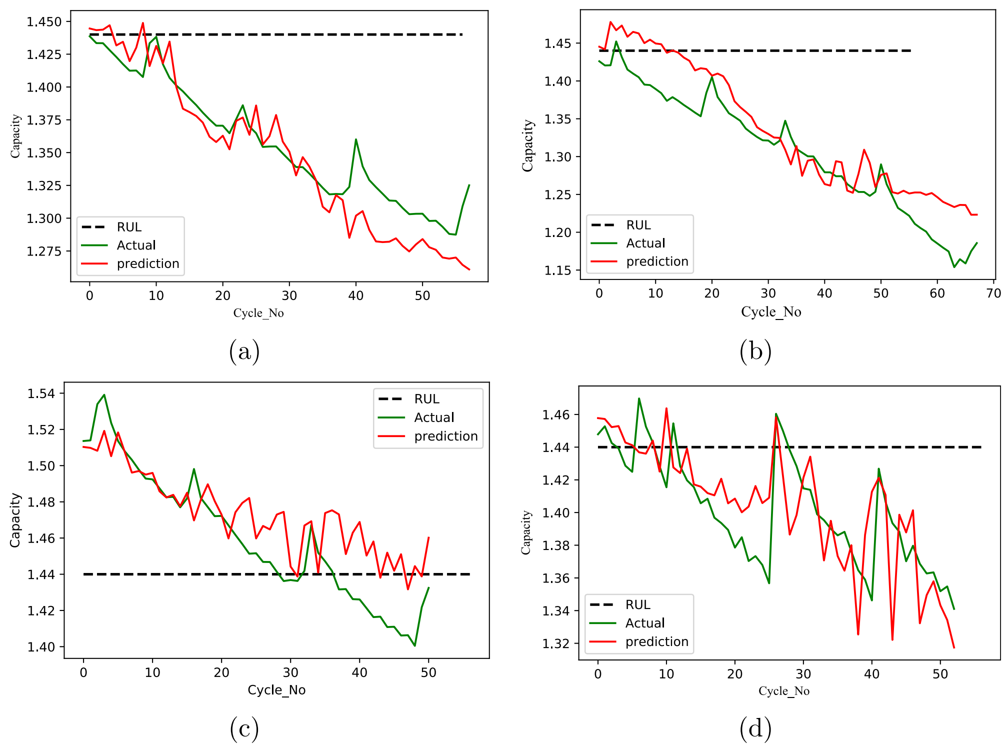

Fig. 13. RUL prediction of different battery models: (a) Battery model B0005, (b) Battery model B0006, (c) Battery model B0007, (d) Battery model B0018. On the vertical axis, the capacity is in Ah unit, and on the horizontal axis, the cycle numbers.

Table 7
Model training time and complexity.

Metric	Value
Training time per epoch	0.00856 s
Number of parameters	22 977
Estimated number of operations in forward pass	80740480.0

dense layers, as the model performs well and does not exhibit an overfitting issue. Table 7 represents the data associated with the proposed model's training time per epoch and computational complexity.

Conclusion

This study presents a novel approach for predicting the RUL of LIBs by combining the Bat optimization technique with a CNN degradation model. This method demonstrates superior performance compared to traditional empirical models, leveraging the CNN model's adaptability to dynamic trends and avoiding sole reliance on degradation patterns. It outperforms traditional deep learning methods and achieves exceptional results with less computational burden and fewer parameters. With an RMSE of 0.0065601 Ah, the approach surpasses other optimizers employing CNN architecture. Additionally, the model achieves an impressive R2 score of 0.998712 and a minimal MAE of 0.004397067 Ah, highlighting its superior performance in RUL estimation.

Moreover, the quantitative evaluation using diverse cycling datasets confirms the effectiveness of the approach in accurately predicting RUL and modeling capacity degradation trends. In Fig. 14, the future research scopes in battery management systems have been illustrated. Looking ahead, future research can explore the practical applications of the prediction method in real-time battery management for electric vehicles, drones, and consumer electronics. Addressing the limitations of operating conditions in dataset availability will be crucial for further enhancing the reliability and applicability of the approach.

Funding

This research was not funded by any institution or company.

CRediT authorship contribution statement

Shahid A. Hasib: Writing – review & editing, Writing – original draft, Visualization, Validation, Software, Resources, Project administration, Methodology, Investigation, Formal analysis, Data curation, Conceptualization. **S. Islam:** Writing – original draft, Methodology, Data curation, Conceptualization. **Md F. Ali:** Supervision. **Subrata. K. Sarker:** Writing – review & editing, Formal analysis. **Li Li:** Writing – review & editing. **Md Mehedi Hasan:** Writing – review & editing, Supervision. **Dip K. Saha:** Writing – review & editing, Writing – original draft, Supervision, Project administration, Investigation, Formal analysis.

Declaration of competing interest

The authors declare that they have no known competing financial interests or personal relationships that could have appeared to influence the work reported in this paper.

Data availability

The datasets used in this research are collected from the NASA Prognostics Center of Excellence (PCoE) data repository.

Link: https://phm-datasets.s3.amazonaws.com/NASA/5.+Battery+Data+Set.zip.

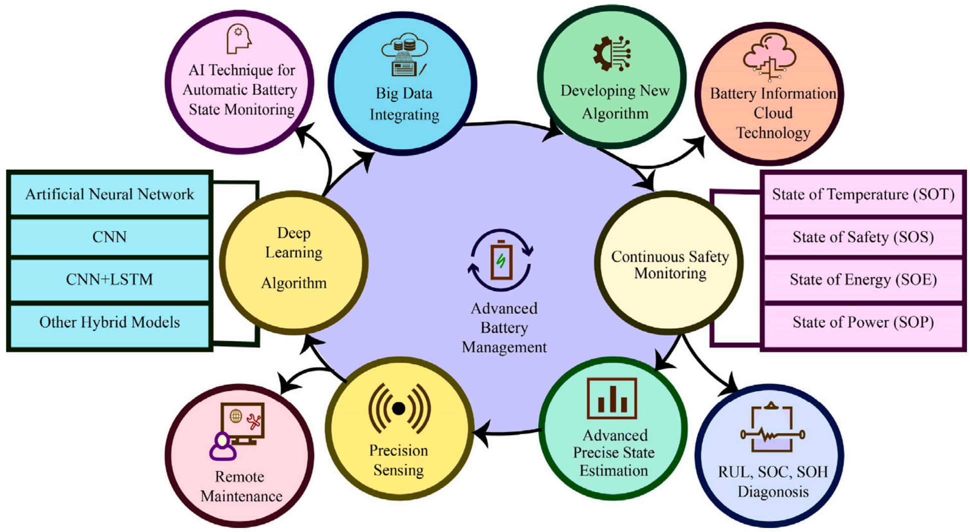

Fig. 14. Future research scopes in battery management.

Table 8
RUL prediction result in comparison for different deep learning algorithms.

Algorithm	RMSE (Ah)	Publication year	Ref.
GRU-GPR	0.0079	2018	[11]
DCNN	0.01986	2020	[39]
DNN	0.0159	2020	[40]
DCNN-ETL	0.01114	2020	[39]
DCNN-TL	0.01361	2020	[39]
ADLSTM-MC	0.033	2021	[41]
DeTransformer	0.0802	2022	[42]
LSTM-Attention Mechanism.	0.0178	2023	[43]
CLDNN	0.8218	2024	[44]
CEG	0.0136	2024	[45]
CNN + Bat optimization	0.00656%	–	–

Table 9
RUL prediction result in comparison for other CNN models.

Algorithm	Battery model	RMSE (Ah)	MAE (Ah)	R2/ Accuracy	Publication year	Ref.
CEEMDAN-CNN BiLSTM	B0005	0.0166	0.0082	–	2023	[46]
CEEMDAN-CNN BiLSTM	B0006	0.0274	0.0101	–	2023	[46]
CNN-LSTM-DNN	B0005	0.0145	0.00826	0.98313	2021	[47]
CNN-LSTM-DNN	B0006	0.0199	0.00892	0.96096	2021	[47]
CNN-LSTM-DNN	B0007	0.01722	0.01199	0.96900	2021	[47]
CNN-LSTM-DNN	B0018	0.02033	0.00966	0.74686	2021	[47]
Auto-CNN-LSTM	–	4.84	–	0.9516	2020	[48]

References

[1] Y. Liu, J. Sun, Y. Shang, X. Zhang, S. Ren, D. Wang, J. Energy Storage 61 (2023) 106645.
[2] Z. He, M. Gao, C. Wang, L. Wang, Y. Liu, Energies 6 (8) (2013) 4134–4151.
[3] Y. Zhang, R. Xiong, H. He, M. Pecht, J. Clean. Prod. 212 (2019) 240–249.
[4] Y. Han, C. Li, L. Zheng, G. Lei, L. Li, Energies 16 (17) (2023) 6328.
[5] K. Javed, R. Gouriveau, N. Zerhouni, Mech. Syst. Signal Process. 94 (2017) 214–236.
[6] R. Kumar, K. Das, Sustain. Energy Technol. Assess. 65 (2024) 103766.
[7] P.K. Koorata, S. Panchal, R. Fraser, M. Fowler, Kausthubharam, J. Energy Storage 84 (2024) 110928.
[8] D. Arora, A. El-Sharkawy, S. Panchal, Development of Time-Temperature Analysis Algorithm for Estimation of Lithium-Ion Battery Useful Life, Tech. Rep. No. 2024-01-2191, SAE Technical Paper, 2024.
[9] Y. Xie, Y. Fan, R. Yang, K. Zhang, B. Chen, S. Panchal, Y. Zhang, IEEE Trans. Transp. Electrif. (2024) 1.
[10] V. Talele, M.S. Patil, U. Moralı, S. Panchal, R. Fraser, M. Fowler, P. Thorat, SAE Int. J. Electrif. Veh. 13 (14-13-03-0017) (2023).
[11] M.H. Lipu, M. Hannan, A. Hussain, M. Hoque, P.J. Ker, M.M. Saad, A. Ayob, J. Clean. Prod. 205 (2018) 115–133.
[12] Y. Chang, H. Fang, Y. Zhang, Appl. Energy 206 (2017) 1564–1578.
[13] M. Pan, P. Hu, R. Gao, K. Liang, Int. J. Green Energy 20 (4) (2023) 408–422.
[14] Z. Liu, G. Sun, S. Bu, J. Han, X. Tang, M. Pecht, IEEE Trans. Instrum. Meas. 66 (2) (2016) 280–293.
[15] M. Al-Greer, I. Bashir, M. El-Dalahmeh, Measurement 214 (2023) 112838.
[16] Y. Zhang, L. Chen, Y. Li, X. Zheng, J. Chen, J. Jin, J. Energy Storage 44 (2021) 103245.
[17] C. Sun, M. Gao, F. Xu, C. Zhu, H. Cai, Data-Driven State-of-Charge Estimation of a Lithium-Ion Battery Pack in Electric Vehicles Based on Real-World Driving Data, Available at SSRN 4737800.
[18] J. Chen, P. Kollmeyer, S. Panchal, Y. Masoudi, O. Gross, A. Emadi, Sequence Training and Data Shuffling to Enhance the Accuracy of Recurrent Neural Network Based Battery Voltage Models, Tech. Rep. No. 2024-01-2426, SAE Technical Paper, 2024.
[19] L. Chen, Y. Ding, B. Liu, S. Wu, Y. Wang, H. Pan, Energy 244 (2022) 122581.
[20] S. Vashisht, D. Rakshit, S. Panchal, M. Fowler, R. Fraser, Electrochemical Society Meeting Abstracts 244, no. 3, The Electrochemical Society, Inc., 2023, p. 445.

[21] J. Li, Highlights Sci. Eng. Technol. 83 (2024) 232–241.
[22] M.-K. Tran, A. DaCosta, A. Mevawalla, S. Panchal, M. Fowler, Batteries 7 (3) (2021) 51.
[23] M. Reza, M. Mannan, M. Mansor, P.J. Ker, T.I. Mahlia, M. Hannan, Energy Rep. 11 (2024) 4824–4848.
[24] J.-H. Seo, M.S. Patil, S. Panchal, M.-Y. Lee, Symmetry 12 (10) (2020) 1713.
[25] X.-S. Yang, Nature Inspired Cooperative Strategies for Optimization, NICSO 2010, Springer, 2010, pp. 65–74.
[26] Y. Wu, W. Li, Y. Wang, K. Zhang, IEEE Access 7 (2019) 54843–54854.
[27] Y. Lian, J.V. Wang, X. Deng, J. Kang, G. Zhu, K. Xiang, 2020 IEEE International Symposium on Circuits and Systems, ISCAS, IEEE, 2020, pp. 1–5.
[28] N. Ames, NASA prognostics center of excellence data repository, 2012.
[29] S.A. Hasib, S. Islam, R.K. Chakrabortty, M.J. Ryan, D.K. Saha, M.H. Ahamed, S.I. Moyeen, S.K. Das, M.F. Ali, M.R. Islam, Z. Tasneem, F.R. Badal, IEEE Access 9 (2021) 86166–86193.
[30] T. Sun, L. Sun, D.-Y. Yeung, Image Vis. Comput. 64 (2017) 47–66.
[31] S. Kiranyaz, T. Ince, M. Gabbouj, IEEE Trans. Biomed. Eng. 63 (3) (2015) 664–675.
[32] W. Gao, J.L. Guirao, B. Basavanagoud, J. Wu, Inform. Sci. 467 (2018) 35–58.
[33] A.A. Heidari, S. Mirjalili, H. Faris, I. Aljarah, M. Mafarja, H. Chen, Fut. Gener. Comput. Syst. 97 (2019) 849–872.
[34] X.-S. Yang, X. He, Int. J. Bio-Inspired Comput. 5 (3) (2013) 141–149.
[35] J. Eklöf, J. Rydell, Bats: In a World of Echoes, Springer, 2018.
[36] A.H. Gandomi, X.-S. Yang, J. Comput. Sci. 5 (2) (2014) 224–232.
[37] L. Chen, J. An, H. Wang, M. Zhang, H. Pan, Energy Rep. 6 (2020) 2086–2093.
[38] L. Zhang, Z. Mu, C. Sun, IEEE Access 6 (2018) 17729–17740.
[39] S. Shen, M. Sadoughi, M. Li, Z. Wang, C. Hu, Appl. Energy 260 (2020) 114296.
[40] X. Cong, C. Zhang, J. Jiang, W. Zhang, Y. Jiang, IEEE Trans. Veh. Technol. 69 (11) (2020) 12775–12785.
[41] Z. Tong, J. Miao, S. Tong, Y. Lu, J. Clean. Prod. 317 (2021) 128265.
[42] D. Chen, W. Hong, X. Zhou, IEEE Access 10 (2022) 19621–19628.
[43] C. Chen, J. Wei, Z. Li, Processes 11 (8) (2023) 2333.
[44] A. Rastegarparnah, M.E. Asif, R. Stolkin, Batteries 10 (3) (2024) 106.
[45] Y. Liu, B. Hou, M. Ahmed, Z. Mao, J. Feng, Z. Chen, Appl. Energy 358 (2024) 122555.
[46] X. Guo, K. Wang, S. Yao, G. Fu, Y. Ning, Energy Rep. 9 (2023) 1299–1306.
[47] B. Zraibi, C. Okar, H. Chaoui, M. Mansouri, IEEE Trans. Veh. Technol. 70 (5) (2021) 4252–4261.
[48] L. Ren, J. Dong, X. Wang, Z. Meng, L. Zhao, M.J. Deen, IEEE Trans. Ind. Inform. 17 (5) (2020) 3478–3487.